Science of the Total Environment 782 (2021) 146918

Contents lists available at ScienceDirect

Science of the Total Environment

journal homepage: www.elsevier.com/locate/scitotenv

Effect of COVID-19 shutdown on aerosol direct radiative forcing over the Indo-Gangetic Plain outflow region of the Bay of Bengal

Abin Thomas [a], Vijay P. Kanawade [a,*], Chandan Sarangi [b,c], Atul K. Srivastava [d]

[a] Centre for Earth, Ocean and Atmospheric Sciences, University of Hyderabad, India
[b] Department of Civil Engineering, Indian Institute of Technology Madras, Chennai, India
[c] Laboratory for Atmospheric and Climate Sciences, Indian Institute of Technology Madras, Chennai, India
[d] Indian Institute of Tropical Meteorology, Ministry of Earth Sciences, New Delhi, India

HIGHLIGHTS

- Direct indication of anthropogenic impact on ADRF over the IGP outflow region of the BoB
- ADRF over the BoB is higher when the winds originated from the IGP.
- COVID-19 shutdown reflected ~20–25% reduction in ADRF over the IGP outflow region.

GRAPHICAL ABSTRACT

The aerosol direct radiative forcing over the Bay of Bengal (BoB) is much higher in magnitude when the winds originate from Indo-Gangetic Plains during the pre-monsoon season (March–May) compared to the seasonal average.

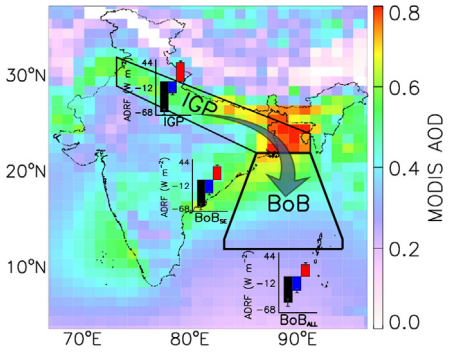

ARTICLE INFO

Article history:
Received 9 December 2020
Received in revised form 13 March 2021
Accepted 30 March 2021
Available online 6 April 2021

Editor: Philip K. Hopke

Keywords:
Continental transport, outflow
Aerosol direct radiative forcing
COVID-19
Indo-Gangetic Plains

ABSTRACT

The Indo Gangetic Plain (IGP), one of the most densely populated regions of the world, is a global hotspot of anthropogenic aerosol emissions. In the pre-monsoon season (March–May), the strong westerlies carry transported dust aerosols along with anthropogenic aerosols onto the Bay of Bengal (BoB). The outflow from IGP modulates the aerosol loading and the aerosol direct radiative forcing (ADRF) over the BoB. The quantification of the anthropogenic aerosol impact on the radiative forcing over the outflow region remains inadequate. The enforced shutdown amid the COVID-19 pandemic eased the anthropogenic activities across the country, which helped to examine the magnitude and variability of aerosol loading and subsequent changes in ADRF over IGP and the outflow region of the BoB. Wind trajectory analysis illustrates that the ADRF over the BoB is greater during the days when the winds originated from the IGP region (at the surface -54.2 ± 6.4 W m^{-2}, at the top of the atmosphere, -26.9 ± 3.4 W m^{-2} and on the atmosphere, 27.0 ± 3.1 W m^{-2}) compared to the seasonal average (-46.3 ± 7.1 W m^{-2}, -24.9 ± 4.0 W m^{-2} and 20.6 ± 3.2 W m^{-2}, respectively). This indicates that anthropogenic aerosols emission from IGP can contribute an additional 31% of the atmospheric ADRF over the IGP outflow region of the BoB. The reduced aerosol loading during the shutdown period resulted in a reduction of ADRF at the surface, at the top of the atmosphere, and on the atmosphere over the IGP outflow region of the BoB by 22.0 ± 3.1%, 20.9 ± 3.4% and 23.2 ± 3.3%, respectively. This resultant 20–25% reduction in ADRF over the IGP outflow region of BOB matches well with 10–25% reduction in aerosol optical depth (AOD) over the IGP during the shutdown period showing a robust coupling between IGP aerosol emissions and ADRF over the BoB.

* Corresponding author.
E-mail address: vijaykanawade03@yahoo.co.in (V.P. Kanawade).

https://doi.org/10.1016/j.scitotenv.2021.146918
0048-9697/

1. Introduction

The global net radiative forcing due to aerosols is negative (IPCC, 2013) and estimated to offset about one-third of the atmospheric warming due to greenhouse gases since the 1950s (Storelvmo et al., 2016). However, the uncertainties in the net aerosol forcing estimates remain due to the complex feedback mechanisms and spatio-temporal variability (Bellouin et al., 2020; Bender, 2020; Li et al., 2009). The South Asian region, especially the Indo-Gangetic plain (IGP) in northern India, is a global pollution hotspot due to a variety of natural and anthropogenic emissions of aerosols (Brooks et al., 2019; Dey et al., 2004; Rana et al., 2019; Singh et al., 2017; Srivastava et al., 2020; Srivastava et al., 2012a). The aerosol loading over the Indian subcontinent and surrounding marine regions has been on the rise due to anthropogenic emissions (Babu et al., 2013; Hsu et al., 2012; Krishna Moorthy et al., 2013; Kumar et al., 2018; Mehta et al., 2021; Srivastava, 2017; Thomas et al., 2019). The IGP region has been the focus in many studies due to high aerosol loading, strong seasonal variability of aerosol composition, complex mixing processes, and its outflow into the Bay of Bengal (BoB) (Nair et al., 2017; Srinivas and Sarin, 2013; Srinivas and Sarin, 2014). The pre-monsoon season (March–May) is marked by an increment in the coarse mode aerosols over north India due to mineral dust advection by the westerly winds (Beegum et al., 2008; Srivastava et al., 2014). The western IGP is more influenced by the dust, and central to eastern IGP has a dominance of anthropogenic aerosols due to coal-based power plants, vehicular emissions, agricultural burning (Gautam et al., 2011; Gogoi et al., 2020; Tobler et al., 2020).

Aerosols in this region come from a complex mixture of sources and include absorbing aerosols like black carbon (BC), brown carbon, dust, and secondary aerosol production (Srivastava et al., 2021b). The mixing of aerosol species and the complexity associated with it makes it difficult to constrain the aerosol properties, and therefore to estimate the direct radiative forcing and climate impacts of aerosols in this region (Kompalli et al., 2020; Srivastava et al., 2020; Srivastava et al., 2018; Thamban et al., 2017). The vertical distribution of aerosols during the pre-monsoon season shows two distinct aerosol layers; a surface layer where the extinction coefficient decreases with altitude and an elevated dust layer mixed with anthropogenic aerosols between 1.5 km to 5.5 km (Brooks et al., 2019; Sarangi et al., 2016; Srivastava et al., 2012b). This elevated layer is known to alter the monsoon circulation via the 'elevated heat pump' leading to an early onset of the monsoon (Lau and Kim, 2006; Menon et al., 2002; Nigam and Bollasina, 2010).

The westerly winds in the pre-monsoon season result in an outflow of dust and anthropogenic aerosols from IGP onto the BoB (Banerjee et al., 2019; Lelieveld et al., 2001; Moorthy et al., 2009; Ramanathan et al., 2001). The outflow from IGP influences the aerosol composition and direct radiative forcing by transporting anthropogenic aerosols as far as southern BoB with a strong north-south gradient (Nair et al., 2013a; Nair et al., 2009; Rastogi et al., 2020; Satheesh et al., 2006). Satellite vertical profiles over the BoB during the pre-monsoon has shown that dust from continental region accounts for 22% of the total aerosol extinction, but the long-term (2006–17) trend shows a decrease in dust aerosols over the BoB (Lakshmi et al., 2017). The winter outflow is dominated by BC and OC aerosols due to fossil fuel and biomass burning from IGP (Bikkina et al., 2016). This influx of aerosols is a source of nutrients over the BoB region and is known to influence the primary productivity over the region for this 4-5 month period (Nair et al., 2013b; Srinivas et al., 2015). The north-eastern BoB is found to have an aerosol-induced atmospheric heating rate as high as ~0.5 K/day during pre-monsoon season due to the influence of anthropogenic aerosols, which could affect the regional circulation (Nair et al., 2013a). The outflow is known to influence the warm clouds with low liquid water path (LWP) over the northern Indian Ocean, causing a warming effect in the region (Jose et al., 2020).

COVID-19 global pandemic has led countries around the world to enforce lockdown (shutdown of anthropogenic activities and movement of peoples) to contain the spread of the virus. The decline in traffic and industrial production has led to a decrease in emission of greenhouse gases, aerosol loading and an overall improvement of air quality in major cities around the globe (Chauhan and Singh, 2020; Muhammad et al., 2020; Singh and Chauhan, 2020). In India, the lockdown was announced in 4 different phases; phase-1: 24 March–14 April, phase-2: 15 April–3 May, phase-3: 4 May–17 May and phase-4: 18 May–31 May 2020. Phase 1 and 2 were the strictest, and the country came to an almost standstill in this period, with all services shutdown except essential transportation and services (e.g., Hospitals). The average $PM_{2.5}$ concentration dropped by about 43% in measurement sites all over India during phase1 and 2 as compared to the previous years (Sharma et al., 2020). Another study reported a drop in the average air quality index (AQI) from ~135 to ~110 in the last week of March 2020 when the lockdown initiated, and similar improvements were reported over other cities in India (Singh and Chauhan, 2020). Mahato et al. (2020) reported a reduction of ~50% in particulate matter (PM) during lockdown (24 March – 31 May) over Delhi as compared to the pre-lockdown time period (1–23 March 2020). AOD and absorption AOD showed a reduction of ~30% over the IGP during COVID-19 shutdown, with concentrations of PM_{10}, $PM_{2.5}$, NO, NO_2 and CO lower by about 58%, 47%, 76%, 68% and 58%, respectively, at Delhi (Srivastava et al., 2021a). The obvious reduction in anthropogenic emissions due to the enforced lockdown amid the COVID-19 pandemic has given unique opportunity to observe the change in ADRF at the outflow region from the IGP in the absence/reduction of anthropogenic emissions. Here, we examine the effect of the COVID-19 shutdown on the ADRF over the Indo-Gangetic Plain outflow region of the BoB during pre-monsoon season. It is to be noted that the change in meteorology and atmospheric dynamics can further complicate the behaviour of aerosols (Guttikunda et al., 2019).

2. Data and methods

2.1. MODIS

The Moderate-resolution imaging spectroradiometer sensor (MODIS) measures the reflectance from the earth's surface in 36 channels in the wavelength range of 0.41–14.4 μm (Remer et al., 2005). The sensor is onboard the EOS-AQUA satellite and crosses the equator at 13:30 local time. In this study, we have used the level-3 Dark Target and Deep Blue combined AOD of collection 6.1 at 0.55 μm with a grid resolution of 1° × 1° (Hsu et al., 2013; Levy et al., 2013; Sayer et al., 2014). Mhawish et al. (2017) evaluated the MODIS AOD against AERONET sites over the IGP and found that the combined Dark Target and Deep Blue algorithm has better accuracy than individual algorithms.

2.2. OMI

The Ozone Measuring Instrument onboard the EOS-AURA satellite has a nadir viewing spectrometer, which measures in UV–visible range (264–504 nm). The OMAERUV algorithm uses 354 and 388 nm reflectance to derive aerosol absorption optical depth (AAOD) at 388 nm (Curier et al., 2008; Torres et al., 2013; Torres et al., 2007). The AAOD at 1° × 1° resolution is available from OMAERUVd.003 product. The daily tropospheric column NO_2 at 0.25° × 0.25° resolution was used in the study. Irie et al. (2008a) describe the retrieval algorithm for the tropospheric NO_2 column, and the validation study showed a bias of 20% globally (Irie et al., 2008b). The daily AAOD and tropospheric NO_2 column are downloaded from the NASA Goddard Earth Sciences, Data and Information Services Center website (http://disc.sci.gsfc.nasa.gov).

2.3. MERRA-2

The Modern-Era Retrospective Analysis for Research and Application version 2 (MERRA-2) was released by the Global Modelling and Assimilation Office (Gelaro et al., 2017). It uses Goddard Earth Observing

System-5 (GEOS-5) atmospheric general circulation model for climate analysis (Molod et al., 2015) and is coupled with the Goddard Global Ozone Chemistry Aerosol Radiation and Transport model (GOCART). The aerosol and meteorological parameters are assimilated in conjunction after careful cloud screening and homogenization of multiple satellite AOD (MODIS, AVHRR and MISR) inputs with and ground-based (AERONET) AOD data (Buchard et al., 2017; Randles et al., 2017). The radiative fluxes data from MERRA-2 was evaluated against CERES EBAF Edition 2.8 satellite product over 2001–2015, and the MERRA-2 radiative fluxes were able to capture the global trends and variability during the period of study (Hinkelman, 2019). The AOD from 'M2I3NXGAS' product and radiation fluxes from 'M2T1NXRAD' product was used in the analysis. Both the products were temporally collocated to match with the overpass time of EOS-AQUA satellite. The data at a grid resolution of 1° × 1° was downloaded from NASA Goddard Earth Sciences (GES) Data and Information Services Center (DISC) https://disc.gsfc.nasa.gov/.

The clear-sky aerosol direct radiative forcing (ADRF) is calculated from the radiative fluxes (shortwave and longwave) by taking the difference between the fluxes in clear-sky conditions with aerosols and without aerosol. The hourly variables; SWGNTCLR (surface net downward shortwave flux assuming clear-sky), SWGNTCLRCLN (surface net downward shortwave flux assuming clear-sky and no aerosol), LWGNTCLR (surface net downward longwave flux assuming clear sky) and LWGNTCLRCLN (surface net downward longwave flux assuming clear-sky and no aerosol) are used to calculate ADRF at the surface ($ADRF_{SURF}$). Concurrently, ADRF at the top of the atmosphere ($ADRF_{TOA}$) is calculated from hourly variables, SWTNTCLR (TOA net downward shortwave flux assuming clear sky), SWTNTCLRCLN (TOA net downward shortwave flux assuming clear-sky and no aerosol), LWTUPCLR (upwelling longwave flux at TOA assuming clear-sky) and LWTUPCLRCLN (upwelling longwave flux at TOA assuming clear-sky and no aerosol).

$$ADRF_{SUR} = (SWGNTCLR + LWGNTCLR) - (SWGNTCLRCLN + LWGNTCLRCLN)$$

$$ADRF_{TOA} = (SWTNTCLR + LWTUPCLR) - (SWTNTCLRCLN + LWTUPCLRCLN)$$

The ADRF on the atmosphere ($ADRF_{ATM}$), which indicates the energy trapped by all aerosols in the atmosphere, is calculated by taking the difference between $ADRF_{TOA}$ and $ADRF_{SURF}$.

2.4. HYSPLIT model

The Hybrid Single Particle Lagrangian Integrated Trajectory (HYSPLIT) Model is extensively used to compute air mass forward trajectories (Rolph et al., 2017; Stein et al., 2016). The PC-based version of the model developed by the NOAA air resources laboratory with Global Data assimilation system (GDAS) 1° × 1° meteorology data as the input is used in this study. The forward trajectories simulated by the model from Kolkata (22.57°N, 88.42°E) were used to identify the days in the pre-monsoon season with trajectories towards the Bay of Bengal. The trajectories were calculated at 00 h UTC (05:30 local time) and at two altitude levels 500 m and 1500 m above the ground. The model was also run from Kanpur (26.28°N, 80.21°E) to establish the general flow of the air mass through IGP in this season (Fig. S1).

2.5. Data analysis

The satellite retrievals are used in conjunction with the reanalysis data products to understand the anthropogenic impact on the ADRF over the IGP and also over the BoB associated with the outflow from IGP. The five-year average (2015–19) during the pre-monsoon season (March to May) is compared with the days when trajectories are towards southeast from Kolkata flowing into the BoB and the days when trajectories are flowing in other directions. The region of interest is marked in Fig. 1a as IGP and BoB based on the airmass trajectory flow as shown in Fig. 2.

3. Results and discussions

3.1. Average aerosol conditions during pre-monsoon

Fig. 1 shows the five-year (2015–2019) averaged MODIS AOD, MERRA-2 AOD, OMI AAOD, and OMI retrieved tropospheric NO_2 column for the pre-monsoon (March–May) season. AOD, as observed by MODIS AQUA (Fig. 1a) and the MERRA-2 AOD (Fig. 1b) compared well and were the highest across the IGP, mainly in the eastern part. The OMI AAOD was also showed high values over IGP and northern BoB (Fig. 1c). The tropospheric NO_2 column shows elevated anthropogenic emission sources over IGP (Fig. 1d). The pre-monsoon season has the highest AOD over IGP due to local emissions and dust transport from north-westerly winds. The eastern IGP is influenced more by anthropogenic aerosols (Gogoi et al., 2020), which was substantiated by the high column NO_2 concentration. Even with the rise in population and industrialization, the trend of total aerosol loading during the pre-monsoon season was found to be insignificant over the IGP region due to the dust influx (Babu et al., 2013). The dust influx over the IGP is known to overshadow the diurnal pattern of local anthropogenic aerosol emissions during the pre-monsoon season and increases the aerosol loading by about 50% (Dey et al., 2004). But a recent study shows that the dust influx over the IGP region during the pre-monsoon has reduced by 10–20% in recent years (Pandey et al., 2017).

The pre-monsoon season is the time of reversal of wind direction from winter to summer. The wind is predominantly westerly over the Indian landmass, and the wind speed increases from March to May as the season progresses (Beegum et al., 2008; Satheesh, 2002). Over BoB, this period is marked by an increase in cyclone frequency and moisture in the mid-troposphere (Balaguru et al., 2016; Li et al., 2013), a precursor condition to the onset of monsoon. The wind flow across the Indian Ocean is zonal during this transition period and carries pollution from India's east coast onto the BoB (Niranjan et al., 2007; Satheesh et al., 2010).

In order to analyze the aerosol loading over BoB due to transport from IGP, the HYSPLIT forward trajectories originating from Kolkata at the eastern IGP and Kanpur at the central IGP are calculated (Fig. S1). More than 90% of forward trajectories from both locations are flowing towards the east. The days when the wind flow from Kolkata is directly onto the BoB are identified and are used in further analysis to determine the transport of aerosols into the BoB. The model run at two altitudes from Kolkata is considered in the study as it is located towards the eastern side of IGP (Fig. S1a and S1b). Two different origin heights (500 m and 1500 m) are taken into account to take into account both the surface aerosol layer and the elevated aerosol layer (if any) during the pre-monsoon over IGP (Brooks et al., 2019; Sarangi et al., 2016). Over the IGP, the lower layers of the atmosphere (<1.5 km) have a higher concentration of absorbing aerosol species, and the elevated layer is dominated by dust and other scattering aerosols in the pre-monsoon season (Brooks et al., 2019). The southeastward trajectories that flow directly into the BoB account for ~16% of the trajectories that originate from Kolkata during this period at 500 m, and most of them flow through BoB at an altitude below 2 km (Fig. 2). A similar pattern was also seen for the air mass initiating at 1500 m (Fig. S1). The majority of these southeastward trajectories flow over the eastern side of the BoB, influencing the aerosol loading over the region (Fig. 2).

The days when the trajectories from Kolkata are flowing directly into the BoB are grouped as BoB_{SE} for both 500 m and 1500 m model origin heights. Fig. 2b shows the mean ADRF at the surface, top of the atmosphere, and in the atmosphere over IGP, BoB, and for the days when the trajectories from IGP are onto the BoB region (IGP_{ALL}, BoB_{ALL} and BoB_{SE}). The five-year average of pre-monsoon ADRF derived from the MERRA-2 dataset over IGP is −56.2 ± 5.8 W m^{-2}, −20.1 ± 3.7 W m^{-2}

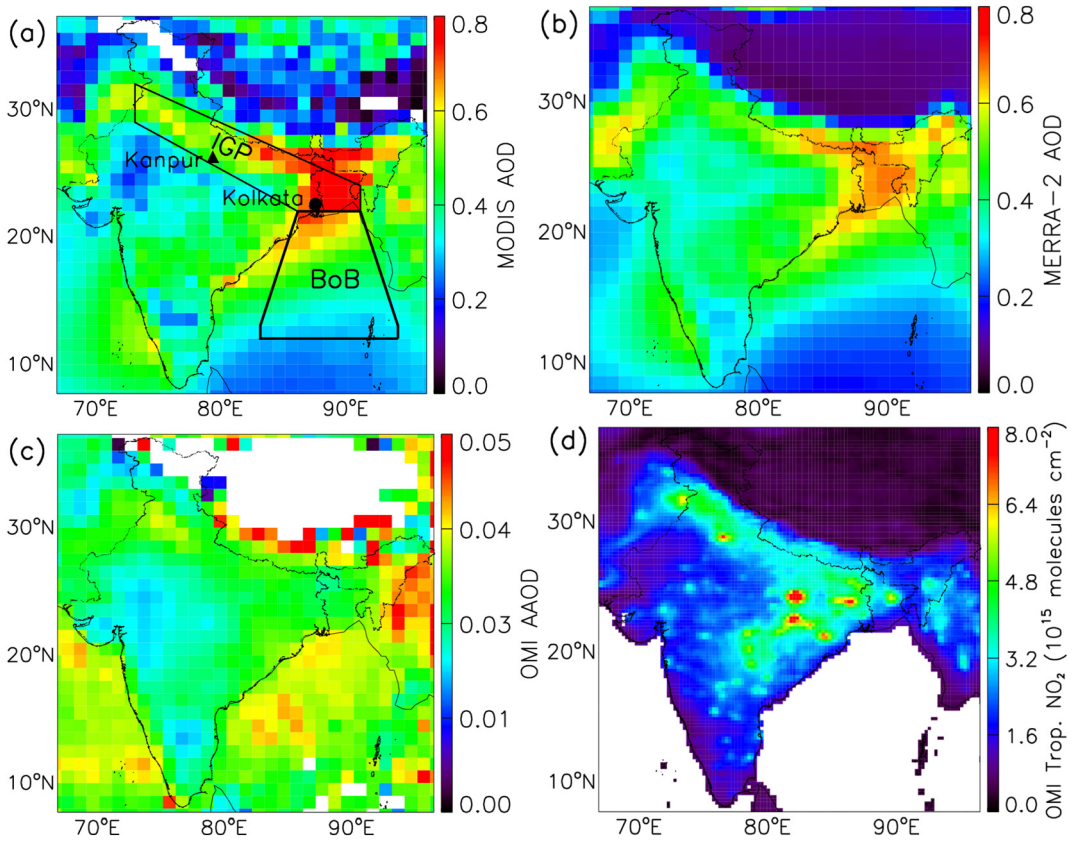

Fig. 1. Averaged (a) MODIS AOD, (b) MERRA-2 AOD, (c) OMI AAOD and (d) OMI tropospheric NO_2 column for the pre-monsoon season (March through May) of 2015–19. The solid triangle and circle symbols indicate the city of Kanpur and Kolkata.

and 35.9 ± 2.9 W m^{-2}, respectively at the surface, top of the atmosphere and in the atmosphere. ADRF corresponding to BoB_{SE} (−54.2 ± 6.4 W m^{-2}, −26.9 ± 3.4 W m^{-2} and 27.0 ± 3.1 W m^{-2}) has the higher magnitude when compared to BoB_{ALL} case (−46.3 ± 7.1 W m^{-2}, −24.9 ± 4.0 Wm^{-2} and 20.6 ± 3.2 W m^{-2}). The difference in the ADRF between BoB_{ALL} and BoB_{SE} (Fig. S2) is more prominent in atmospheric forcing (−27.6 ± 6.8%) than the surface (−14.8 ± 5.2%) or at the top of the atmosphere (−5.7 ± 4.6%). The presence of absorbing aerosols in the lower level transport from IGP is evident from the difference in the atmospheric forcing.

Satheesh (2002) reported a net surface ADRF of −27 W m^{-2} and TOA forcing of −4 W m^{-2} from shipborne observations over the BoB during March 2001. Similarly, the average ADRF over the BoB during the pre-monsoon season of 2006 was observed to be −22.4 W m^{-2}, −12.0 W m^{-2}, and 10.4 W m^{-2}at the surface, top of the atmosphere, and in the atmosphere, respectively (Kedia et al., 2010). Our estimates of the mean ADRF based on the time period of 2015–19 indicates that ADRF over the BoB has doubled in the recent past decade (BoB_{ALL}: −46.3 ± 7.1 W m^{-2}, −24.9 ± 4.0 Wm^{-2}, and 20.6 ± 3.2 W m^{-2}, at the surface, top of the atmosphere, and in the atmosphere, respectively) as compared to the previous study by Kedia et al. (2010).

3.2. COVID-19 shutdown: cleaner atmospheric scenario

The decrease in the aerosol loading and GHGs due to the COVID-19 lockdown has been reported widely around the globe (Chauhan and

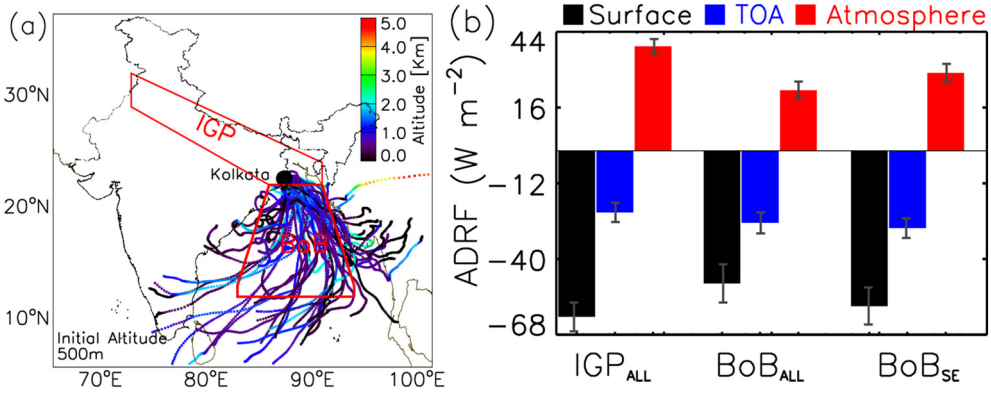

Fig. 2. (a) Five-day forward southeastward trajectories from Kolkata during the pre-monsoon season of 2015–19 with the model start height 500 m above the ground level. The colorbar indicates the altitude of the trajectory. (b) Mean ADRF at the surface, top of the atmosphere and in the atmosphere over IGP and the BoB during pre-monsoon of 2015–2019 and ADRF over the BoB when the southeastward forward trajectories from Kolkata are flowing onto the BoB.

Singh, 2020; Muhammad et al., 2020). The satellite and reanalysis datasets in this study have also shown similar reductions over the Indian region (Fig. 3). The difference is calculated for the pre-monsoon season of 2020 over India against the five-year (2015–19) average of the same time period. In Fig. 3a, MODIS AOD showed a decrease of 17.9 ± 8.5% and 19.1 ± 6.6% over the IGP and BoB, respectively. A slight increment in AOD is observed over central west India can be attributed to the frequent dust storms and transport from the Thar desert (Badarinath et al., 2007; Sikka, 1997) due to the prevailing wind conditions. The reduction in anthropogenic aerosol loading during the lockdown is captured well by the MERRA- 2 reanalysis data products, which are evident from the reduction in total AOD (Fig. 3b). The reduction over IGP is much prominent for OMI - AAOD (35.8 ± 11.3%), showing a significant reduction of absorbing aerosols over the region (Fig. 3c). The OMI tropospheric NO_2 also had a reduction of 8.7 ± 10.2% over the IGP, underlying the reduction in anthropogenic emissions during this period. The cleaner atmospheric condition in the pre-monsoon of 2020 is clearly due to the decrease in emissions that came as a result of the COVID-19 lockdown.

Babu et al. (2008) has shown the existence of BC aerosol layer over northern BoB at an altitude of 2000 m due to transport from the Indian subcontinent. The maximum AOD and BC mass fraction over northern BoB is observed during April–May, and the variation has been matched with that of the East Coast of India (Satheesh et al., 2006). Thus, the reduction in aerosol loading over northern BoB in the present case is also associated with that of the IGP, with reduced emission sources due to COVID-19 shutdown.

The reduction in anthropogenic aerosol loading has led to a decrease in ADRF, as seen in Fig. 4. The reduction in ADRF in the pre-monsoon of 2020 over IGP compared to the average of the previous five years was 17.4 ± 4.9%, 17.2 ± 4.8% and 17.4 ± 5.5% at the surface, TOA and in the atmosphere, respectively. In BoB_{ALL}, this reduction was seen as 19.7 ± 5.3%, 20.9 ± 5.6% and 18.3 ± 5.5% and during BoB_{SE}, it was 22.0 ± 3.1%, 20.9 ± 3.4% and 23.2 ± 3.3%. The reduction in the atmospheric ADRF (~20–25%) during BoB_{SE} is much greater than BoB_{ALL}, highlighting the influence of absorbing aerosol transport from IGP. This 20–25% reduction in the atmospheric forcing due to aerosols in BoB_{SE} matches with the ~10–25% reduction in total AOD and ~24–45% reduction in AAOD over IGP due to the lockdown. This clearly indicates the robust relation of the ADRF over the BoB with the anthropogenic emissions from IGP. The reduction in ADRF over the IGP (~17%) is lower compared to the BoB_{SE} due to the pre-monsoon dust influx over the region, which possibly diluted the overall reduction in aerosol loading (Fig. S3).

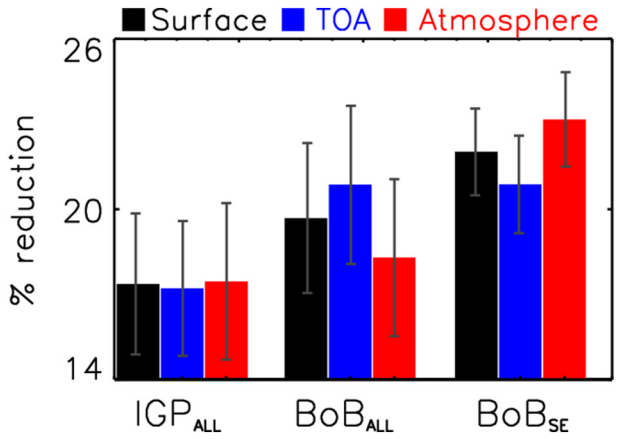

Fig. 4. Percentage difference in the mean ADRF at the surface, top of the atmosphere and in the atmosphere for the pre-monsoon season between 2020 and the five-year average (2015–2019) over Indo-Gangetic Plain and Bay of Bengal. BoB_{SE} indicates the days when Southeast forward trajectories from Kolkata reaching onto BoB.

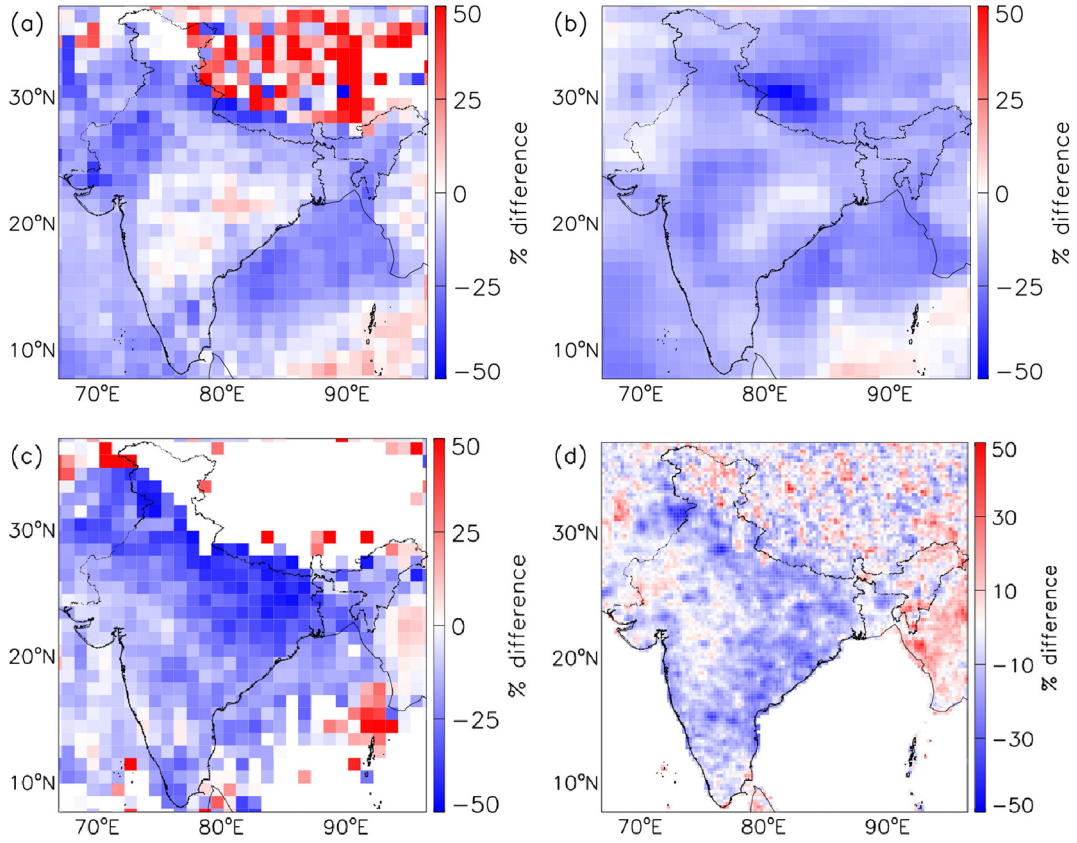

Fig. 3. Percentage difference in (a) MODIS AOD, (b) MERRA-2 AOD, (c) OMI AAOD and (d) OMI tropospheric column NO_2 for the pre-monsoon season between 2020 and five-year average (2015–19).

4. Conclusions

The high aerosol loading over IGP during the pre-monsoon season influences the aerosol composition and thus the ADRF over the BoB due to the prevailing wind pattern. The ADRF calculated from MERRA-2 radiation fluxes over the IGP showed an average value of -56.2 ± 5.8 W m^{-2}, -20.1 ± 3.7 W m^{-2} and 35.9 ± 2.9 W m^{-2}, respectively at the surface, top of the atmosphere and in the atmosphere. The ADRF is high over BoB during the days when the wind trajectories are from the IGP region (-54.2 ± 6.4 W m^{-2}, -26.9 ± 3.4 W m^{-2} and 27.0 ± 3.1 W m^{-2}) compared to the seasonal average (-46.3 ± 7.1 W m^{-2}, -24.9 ± 4.0 Wm^{-2} and 20.6 ± 3.2 W m^{-2}). This shows the influence over aerosol transport from IGP on the ADRF over BoB. The COVID -19 pandemic and the lockdown that followed in order to mitigate the spread of the virus was an unprecedented scenario. The industrial and transportation sectors, which were a significant contributor to the emissions in the polluted IGP, came to an almost halt. This has helped in analyzing the impact of anthropogenic aerosol forcing during the pre-monsoon season, which has a complex aerosol composition due to the mixing of transported natural dust aerosols and local anthropogenic aerosols. Our analysis showed a reduction of ~10–25% in AOD and 24–45% in AAOD over the IGP region. This leads to 20–25% reduction in ADRF over the IGP outflow region of the BOB, and this reduction in ADRF over the BoB is higher when the winds are originating from IGP. The ADRF at the top of the atmosphere, at the surface and on the atmosphere over the BoB reduced by 22.0 ± 3.1%, 20.9 ± 3.4% and 23.2 ± 3.3%, respectively. This implies the robustness of the relation of ADRF over the BoB to the emissions from IGP during the pre-monsoon season. The ADRF change over the BoB can alter the meridional circulation through thermodynamic feedbacks in the atmosphere. The changes in cloud properties and the storms due to the reduced aerosol loading could have a much stronger alteration in the forcing over this region. Our findings warrant more detailed observational and modelling studies to quantify this association as the variability in ADRF over the BoB could influence the monsoon circulation and cyclone genesis by perturbing the land-sea thermal gradients.

CRediT authorship contribution statement

Abin Thomas: Methodology, Formal analysis, Software, Visualization, Validation, Writing – original draft, Writing – review & editing. **Vijay P. Kanawade:** Conceptualization, Methodology, Formal analysis, Writing – review & editing, Supervision. **Chandan Sarangi:** Methodology, Resources, Investigation, Writing – review & editing. **Atul K. Srivastava:** Resources, Investigation, Writing – review & editing.

Declaration of competing interest

The authors declare that they have no known competing financial interests or personal relationships that could have appeared to influence the work reported in this paper.

Acknowledgments and data availability

VPK would like to thank University Grants Commission, Government of India, for UGC Start-Up Grant [Ref. No. F.4-5(230-FRP/2015/BSR)]. AT was supported by University Grants Commission Junior Research Fellowship. CS is supported by the New Faculty Initiation Grant project number CE/20-21/065/NFIG/008961 from Indian Institute of Technology Madras. The authors acknowledge Director, Indian Institute of Tropical Meteorology, Ministry of Earth Sciences, India. The authors acknowledge the use of publicly available data from the NASA Goddard Earth Sciences (GES) Data and Information Services Center (DISC).

MODIS cloud level 3 collection 6.1 is publicly available from LAADS DAAC at https://ladsweb.modaps.eosdis.nasa.gov/missions-and-measurements/science-domain/cloud.

MERRA-2 and OMI data is available at MDISC https://disc.gsfc.nasa.gov/.

Appendix A. Supplementary data

Supplementary data to this article can be found online at https://doi.org/10.1016/j.scitotenv.2021.146918.

References

Babu, S.S., Satheesh, S.K., Moorthy, K.K., Dutt, C.B.S., Nair, V.S., Alappattu, D.P., et al., 2008. Aircraft measurements of aerosol black carbon from a coastal location in the north-east part of peninsular India during ICARB. J. Earth Syst. Sci. 117, 263–271. https://doi.org/10.1007/s12040-008-0030-1.

Babu, S.S., Manoj, M.R., Moorthy, K.K., Gogoi, M.M., Nair, V.S., Kompalli, S.K., et al., 2013. Trends in aerosol optical depth over Indian region: potential causes and impact indicators. J. Geophys. Res. - Atmos. 118, 11,794–11,806. doi:https://doi.org/10.1002/2013jd020507.

Badarinath, K.V.S., Kharol, S.K., Kaskaoutis, D.G., Kambezidis, H.D., 2007. Case study of a dust storm over Hyderabad area, India: its impact on solar radiation using satellite data and ground measurements. Sci. Total Environ. 384, 316–332. https://doi.org/10.1016/j.scitotenv.2007.05.031.

Balaguru, K., Leung, L.R., Lu, J., Foltz, G.R., 2016. A meridional dipole in premonsoon Bay of Bengal tropical cyclone activity induced by ENSO. J. Geophys. Res. - Atmos. 121, 6954–6968. https://doi.org/10.1002/2016jd024936.

Banerjee, P., Satheesh, S.K., Moorthy, K.K., Nanjundiah, R.S., Nair, V.S., 2019. Long-range transport of mineral dust to the Northeast Indian Ocean: regional versus remote sources and the implications. J. Clim. 32, 1525–1549. https://doi.org/10.1175/JCLI-D-18-0403.1.

Beegum, S.N., Moorthy, K.K., Nair, V.S., Babu, S.S., Satheesh, S.K., Vinoj, V., et al., 2008. Characteristics of spectral aerosol optical depths over India during ICARB. J. Earth Syst. Sci. 117, 303–313. https://doi.org/10.1007/s12040-008-0033-y.

Bellouin, N., Quaas, J., Gryspeerdt, E., Kinne, S., Stier, P., Watson-Parris, D., et al., 2020. Bounding global aerosol radiative forcing of climate change. 58, e2019RG000660. Rev. Geophys. doi:https://doi.org/10.1029/2019RG000660.

Bender, F. A-M., 2020. Aerosol forcing: still uncertain, still relevant. AGU Advances. 1, e2019AV000128. doi:https://doi.org/10.1029/2019av000128.

Bikkina, S., Kawamura, K., Sarin, M., 2016. Stable carbon and nitrogen isotopic composition of fine mode aerosols (PM2.5) over the Bay of Bengal: impact of continental sources. Tellus Ser. B Chem. Phys. Meteorol. 68, 31518. https://doi.org/10.3402/tellusb.v68.31518.

Brooks, J., Allan, J.D., Williams, P.I., Liu, D., Fox, C., Haywood, J., et al., 2019. Vertical and horizontal distribution of submicron aerosol chemical composition and physical characteristics across northern India during pre-monsoon and monsoon seasons. Atmos. Chem. Phys. 19, 5615–5634. https://doi.org/10.5194/acp-19-5615-2019.

Buchard, V., Randles, C.A., da Silva, A.M., Darmenov, A., Colarco, P.R., Govindaraju, R., et al., 2017. The MERRA-2 aerosol reanalysis, 1980 onward. Part II: evaluation and case studies. J. Clim. 30, 6851–6872. https://doi.org/10.1175/JCLI-D-16-0613.1.

Chauhan, A., Singh, R.P., 2020. Decline in PM2.5 concentrations over major cities around the world associated with COVID-19. Environ. Res. 187, 109634. https://doi.org/10.1016/j.envres.2020.109634.

Curier, R.L., Veefkind, J.P., Braak, R., Veihelmann, B., Torres, O., de Leeuw, G., 2008. Retrieval of aerosol optical properties from OMI radiances using a multiwavelength algorithm: application to western Europe. J. Geophys. Res. – Atmos. 113. doi:https://doi.org/10.1029/2007jd008738.

Dey, S., Tripathi, S.N., Singh, R.P., Holben, B.N., 2004. Influence of dust storms on the aerosol optical properties over the Indo-Gangetic basin. J. Geophys. Res. – Atmos. 109. doi:https://doi.org/10.1029/2004jd004924.

Gautam, R., Hsu, N.C., Tsay, S.C., Lau, K.M., Holben, B., Bell, S., et al., 2011. Accumulation of aerosols over the Indo-Gangetic plains and southern slopes of the Himalayas: distribution, properties and radiative effects during the 2009 pre-monsoon season. Atmos. Chem. Phys. 11, 12841–12863. https://doi.org/10.5194/acp-11-12841-2011.

Gelaro, R., McCarty, W., Suárez, M.J., Todling, R., Molod, A., Takacs, L., et al., 2017. The Modern-Era Retrospective Analysis for Research and Applications, Version 2 (MERRA-2). J. Clim. 30, 5419–5454. doi:https://doi.org/10.1175/JCLI-D-16-0758.1.

Gogoi, M.M., Jayachandran, V.N., Vaishya, A., Babu, S.N.S., Satheesh, S.K., Moorthy, K.K., 2020. Airborne in situ measurements of aerosol size distributions and black carbon across the Indo-Gangetic Plain during SWAAMI–RAWEX. Atmos. Chem. Phys. 20, 8593–8610. https://doi.org/10.5194/acp-20-8593-2020.

Guttikunda, S.K., Nishadh, K.A., Jawahar, P., 2019. Air pollution knowledge assessments (APnA) for 20 Indian cities. Urban Clim. 27, 124–141. https://doi.org/10.1016/j.uclim.2018.11.005.

Hinkelman, L.M., 2019. The global radiative energy budget in MERRA and MERRA-2: evaluation with respect to CERES EBAF data. J. Clim. 32, 1973–1994. https://doi.org/10.1175/JCLI-D-18-0445.1.

Hsu, N.C., Gautam, R., Sayer, A.M., Bettenhausen, C., Li, C., Jeong, M.J., et al., 2012. Global and regional trends of aerosol optical depth over land and ocean using SeaWiFS measurements from 1997 to 2010. Atmos. Chem. Phys. 12, 8037–8053. https://doi.org/10.5194/acp-12-8037-2012.

Hsu, N.C., Jeong, M.-J., Bettenhausen, C., Sayer, A.M., Hansell, R., Seftor, C.S., et al., 2013. Enhanced Deep Blue aerosol retrieval algorithm: the second generation. J. Geophys. Res. - Atmos. 118, 9296–9315. https://doi.org/10.1002/jgrd.50712.

IPCC, 2013. Climate Change 2013: The Physical Science Basis. Contribution of Working Group I to the Fifth Assessment Report of the Intergovernmental Panel on Climate Change. Cambridge University Press, Cambridge, United Kingdom and New York, NY, USA.

Irie, H., Kanaya, Y., Akimoto, H., Iwabuchi, H., Shimizu, A., Aoki, K., 2008a. First retrieval of tropospheric aerosol profiles using MAX-DOAS and comparison with lidar and sky radiometer measurements. Atmos. Chem. Phys. 8, 341–350. https://doi.org/10.5194/acp-8-341-2008.

Irie, H., Kanaya, Y., Akimoto, H., Tanimoto, H., Wang, Z., Gleason, J.F., et al., 2008b. Validation of OMI tropospheric NO2 column data using MAX-DOAS measurements deep inside the North China Plain in June 2006: Mount Tai Experiment 2006. Atmos. Chem. Phys. 8, 6577–6586. https://doi.org/10.5194/acp-8-6577-2008.

Jose, S., Nair, V.S., Babu, S.S., 2020. Anthropogenic emissions from South Asia reverses the aerosol indirect effect over the northern Indian Ocean. Sci. Rep. 10, 18360. https://doi.org/10.1038/s41598-020-74897-x.

Kedia, S., Ramachandran, S., Kumar, A., Sarin, M.M., 2010. Spatiotemporal gradients in aerosol radiative forcing and heating rate over Bay of Bengal and Arabian Sea derived on the basis of optical, physical, and chemical properties. J. Geophys. Res. – Atmos. 115. doi:https://doi.org/10.1029/2009JD013136.

Kompalli, S.K., Suresh Babu, S.N., Satheesh, S.K., Krishna Moorthy, K., Das, T., Boopathy, R., et al., 2020. Seasonal contrast in size distributions and mixing state of black carbon and its association with PM1.0 chemical composition from the eastern coast of India. Atmos. Chem. Phys. 20, 3965–3985. https://doi.org/10.5194/acp-20-3965-2020.

Kumar, M., Parmar, K.S., Kumar, D.B., Mhawish, A., Broday, D.M., Mall, R.K., et al., 2018. Long-term aerosol climatology over Indo-Gangetic Plain: trend, prediction and potential source fields. Atmos. Environ. 180, 37–50. https://doi.org/10.1016/j.atmosenv.2018.02.027.

Lakshmi, N.B., Nair, V.S., Suresh Babu, S., 2017. Vertical structure of aerosols and mineral dust over the Bay of Bengal from multisatellite observations. J. Geophys. Res. - Atmos. 122, 12,845–12,861. https://doi.org/10.1002/2017JD027643.

Lau, K.-M., Kim, K.-M., 2006. Observational relationships between aerosol and Asian monsoon rainfall, and circulation. Geophys. Res. Lett. 33. https://doi.org/10.1029/2006gl027546.

Lelieveld, J., Crutzen, P.J., Ramanathan, V., Andreae, M.O., Brenninkmeijer, C.A.M., Campos, T., et al., 2001. The Indian Ocean Experiment: widespread air pollution from south and southeast Asia. Science. 291, 1031–1036. https://doi.org/10.1126/science.1057103.

Levy, R.C., Mattoo, S., Munchak, L.A., Remer, L.A., Sayer, A.M., Patadia, F., et al., 2013. The Collection 6 MODIS aerosol products over land and ocean. Atmos. Meas. Tech. 6, 2989–3034. https://doi.org/10.5194/amt-6-2989-2013.

Li, Z., Zhao, X., Kahn, R., Mishchenko, M., Remer, L., Lee, K.H., et al., 2009. Uncertainties in satellite remote sensing of aerosols and impact on monitoring its long-term trend: a review and perspective. Ann. Geophys. 27, 2755–2770. https://doi.org/10.5194/angeo-27-2755-2009.

Li, Z., Yu, W., Li, T., Murty, V.S.N., Tangang, F., 2013. Bimodal character of cyclone climatology in the Bay of Bengal modulated by monsoon seasonal cycle. J. Clim. 26, 1033–1046. https://doi.org/10.1175/JCLI-D-11-00627.1.

Mahato, S., Pal, S., Ghosh, K.G., 2020. Effect of lockdown amid COVID-19 pandemic on air quality of the megacity Delhi, India. Sci. Total Environ. 730, 139086. https://doi.org/10.1016/j.scitotenv.2020.139086.

Mehta, M., Khushboo, R., Raj, R., Singh, N., 2021. Spaceborne observations of aerosol vertical distribution over Indian mainland (2009–2018). Atmos. Environ. 244, 117902. https://doi.org/10.1016/j.atmosenv.2020.117902.

Menon, S., Hansen, J., Nazarenko, L., Luo, Y., 2002. Climate effects of black carbon aerosols in China and India. Science. 297, 2250–2253. https://doi.org/10.1126/science.1075159.

Mhawish, A., Banerjee, T., Broday, D.M., Misra, A., Tripathi, S.N., 2017. Evaluation of MODIS Collection 6 aerosol retrieval algorithms over Indo-Gangetic Plain: implications of aerosols types and mass loading. Remote Sens. Environ. 201, 297–313. https://doi.org/10.1016/j.rse.2017.09.016.

Molod, A., Takacs, L., Suarez, M., Bacmeister, J., 2015. Development of the GEOS-5 atmospheric general circulation model: evolution from MERRA to MERRA2. Geosci. Model Dev. 8, 1339–1356. https://doi.org/10.5194/gmd-8-1339-2015.

Moorthy, K.K., Nair, V.S., Babu, S.S., Satheesh, S.K., 2009. Spatial and vertical heterogeneities in aerosol properties over oceanic regions around India: implications for radiative forcing. Q. J. R. Meteorol. Soc. 135, 2131–2145. https://doi.org/10.1002/qj.525.

Moorthy, K.K., Babu, S.S., Manoj, M.R., Satheesh, S.K., 2013. Buildup of aerosols over the Indian Region. Geophys. Res. Lett. 40, 1011–1014. https://doi.org/10.1002/grl.50165.

Muhammad, S., Long, X., Salman, M., 2020. COVID-19 pandemic and environmental pollution: a blessing in disguise? Sci. Total Environ. 728, 138820. https://doi.org/10.1016/j.scitotenv.2020.138820.

Nair, V.S., Moorthy, K.K., Babu, S.S., Satheesh, S.K., 2009. Optical and physical properties of atmospheric aerosols over the Bay of Bengal during ICARB. J. Atmos. Sci. 66, 2640–2658. https://doi.org/10.1175/2009JAS3032.1.

Nair, V.S., Babu, S.S., Moorthy, K.K., Prijith, S.S., 2013a. Spatial gradients in aerosol-induced atmospheric heating and surface dimming over the oceanic regions around India: anthropogenic or natural? J. Clim. 26, 7611–7621. https://doi.org/10.1175/JCLI-D-12-00616.1.

Nair, V.S., Moorthy, K.K., Babu, S.S., 2013b. Influence of continental outflow and ocean biogeochemistry on the distribution of fine and ultrafine particles in the marine atmospheric boundary layer over Arabian Sea and Bay of Bengal. J. Geophys. Res. - Atmos. 118, 7321–7331. https://doi.org/10.1002/jgrd.50541.

Nair, V.S., Babu, S.S., Manoj, M.R., Moorthy, K.K., Chin, M., 2017. Direct radiative effects of aerosols over South Asia from observations and modeling. Clim. Dyn. 49, 1411–1428. https://doi.org/10.1007/s00382-016-3384-0.

Nigam, S., Bollasina, M., 2010. "Elevated heat pump" hypothesis for the aerosol-monsoon hydroclimate link: "Grounded" in observations? J. Geophys. Res. Atmos. 115. https://doi.org/10.1029/2009jd013800.

Niranjan, K., Madhavan, B.L., Sreekanth, V., 2007. Micro pulse lidar observation of high altitude aerosol layers at Visakhapatnam located on the east coast of India. Geophys. Res. Lett. 34. https://doi.org/10.1029/2006gl028199.

Pandey, S.K., Vinoj, V., Landu, K., Babu, S.S., 2017. Declining pre-monsoon dust loading over South Asia: signature of a changing regional climate. Sci. Rep. 7, 16062. https://doi.org/10.1038/s41598-017-16338-w.

Ramanathan, V., Crutzen, P.J., Lelieveld, J., Mitra, A.P., Althausen, D., Anderson, J., et al., 2001. Indian Ocean Experiment: an integrated analysis of the climate forcing and effects of the great Indo-Asian haze. J. Geophys. Res. - Atmos. 106, 28371–28398. https://doi.org/10.1029/2001jd900133.

Rana, A., Jia, S., Sarkar, S., 2019. Black carbon aerosol in India: a comprehensive review of current status and future prospects. Atmos. Res. 218, 207–230. https://doi.org/10.1016/j.atmosres.2018.12.002.

Randles, C.A., da Silva, A.M., Buchard, V., Colarco, P.R., Darmenov, A., Govindaraju, R., et al., 2017. The MERRA-2 aerosol reanalysis, 1980 onward. Part I: system description and data assimilation evaluation. J. Clim. 30, 6823–6850. https://doi.org/10.1175/JCLI-D-16-0609.1.

Rastogi, N., Agnihotri, R., Sawlani, R., Patel, A., Babu, S.S., Satish, R., 2020. Chemical and isotopic characteristics of PM10 over the Bay of Bengal: effects of continental outflow on a marine environment. Sci. Total Environ. 726, 138438. https://doi.org/10.1016/j.scitotenv.2020.138438.

Remer, L.A., Kaufman, Y.J., Tanré, D., Mattoo, S., Chu, D.A., Martins, J.V., et al., 2005. The MODIS aerosol algorithm, products, and validation. J. Atmos. Sci. 62, 947–973. https://doi.org/10.1175/JAS3385.1.

Rolph, G., Stein, A., Stunder, B., 2017. Real-time Environmental Applications and Display sYstem: READY. Environ. Model. Softw. 95, 210–228. https://doi.org/10.1016/j.envsoft.2017.06.025.

Sarangi, C., Tripathi, S.N., Mishra, A.K., Goel, A., Welton, E.J., 2016. Elevated aerosol layers and their radiative impact over Kanpur during monsoon onset period. J. Geophys. Res. - Atmos. 121, 7936–7957. https://doi.org/10.1002/2015jd024711.

Satheesh, S.K., 2002. Radiative forcing by aerosols over Bay of Bengal region. Geophys. Res. Lett. 29, 40-1–40-4. https://doi.org/10.1029/2002gl015334.

Satheesh, S.K., Srinivasan, J., Moorthy, K.K., 2006. Spatial and temporal heterogeneity in aerosol properties and radiative forcing over Bay of Bengal: sources and role of aerosol transport. J. Geophys. Res. Atmos. 111. https://doi.org/10.1029/2005jd006374.

Satheesh, S.K., Vinoj, V., Krishnamoorthy, K., 2010. Assessment of aerosol radiative impact over oceanic regions adjacent to Indian subcontinent using multisatellite analysis. Adv. Meteorol. 2010, 139186. doi:https://doi.org/10.1155/2010/139186.

Sayer, A.M., Munchak, L.A., Hsu, N.C., Levy, R.C., Bettenhausen, C., Jeong, M.-J., 2014. MODIS Collection 6 aerosol products: comparison between Aqua's e-Deep Blue, Dark Target, and "merged" data sets, and usage recommendations. J. Geophys. Res. Atmos 119, 13,965–13,989. https://doi.org/10.1002/2014jd022453.

Sharma, S., Zhang, M., Anshika, Gao, J., Zhang, H., Kota, S.H., 2020. Effect of restricted emissions during COVID-19 on air quality in India. Sci. Total Environ. 728, 138878. https://doi.org/10.1016/j.scitotenv.2020.138878.

Sikka, D.R., 1997. Desert climate and its dynamics. Curr. Sci. 72, 35–46.

Singh, R.P., Chauhan, A., 2020. Impact of lockdown on air quality in India during COVID-19 pandemic. Air Qual. Atmos. Health 13, 921–928. https://doi.org/10.1007/s11869-020-00863-1.

Singh, N., Mhawish, A., Deboudt, K., Singh, R.S., Banerjee, T., 2017. Organic aerosols over Indo-Gangetic Plain: sources, distributions and climatic implications. Atmos. Environ. 157, 59–74. https://doi.org/10.1016/j.atmosenv.2017.03.008.

Srinivas, B., Sarin, M.M., 2013. Light absorbing organic aerosols (brown carbon) over the tropical Indian Ocean: impact of biomass burning emissions. Environ. Res. Lett. 8, 044042. https://doi.org/10.1088/1748-9326/8/4/044042.

Srinivas, B., Sarin, M.M., 2014. Brown carbon in atmospheric outflow from the Indo-Gangetic Plain: mass absorption efficiency and temporal variability. Atmos. Environ. 89, 835–843. https://doi.org/10.1016/j.atmosenv.2014.03.030.

Srinivas, B., Sarin, M.M., Sarma, V.V.S.S., 2015. Atmospheric outflow of nutrients to the Bay of Bengal: impact of anthropogenic sources. J. Mar. Syst. 141, 34–44. https://doi.org/10.1016/j.jmarsys.2014.07.008.

Srivastava, R., 2017. Trends in aerosol optical properties over South Asia. Int. J. Climatol. 37, 371–380. https://doi.org/10.1002/joc.4710.

Srivastava, A.K., Singh, S., Tiwari, S., Bisht, D.S., 2012a. Contribution of anthropogenic aerosols in direct radiative forcing and atmospheric heating rate over Delhi in the Indo-Gangetic Basin. Environ. Sci. Pollut. Res. 19, 1144–1158. https://doi.org/10.1007/s11356-011-0633-y.

Srivastava, A.K., Singh, S., Tiwari, S., Kanawade, V.P., Bisht, D.S., 2012b. Variation between near-surface and columnar aerosol characteristics during the winter and summer at Delhi in the Indo-Gangetic Basin. J. Atmos. Sol. Terr. Phys. 77, 57–66. https://doi.org/10.1016/j.jastp.2011.11.009.

Srivastava, A.K., Soni, V.K., Singh, S., Kanawade, V.P., Singh, N., Tiwari, S., et al., 2014. An early South Asian dust storm during March 2012 and its impacts on Indian Himalayan foothills: a case study. Sci. Total Environ. 493, 526–534. https://doi.org/10.1016/j.scitotenv.2014.06.024.

Srivastava, P., Dey, S., Srivastava, A.K., Singh, S., Tiwari, S., 2018. Most probable mixing state of aerosols in Delhi NCR, northern India. Atmos. Res. 200, 88–96. https://doi.org/10.1016/j.atmosres.2017.09.018.

Srivastava, A.K., Mehrotra, B.J., Singh, A., Singh, V., Bisht, D.S., Tiwari, S., et al., 2020. Implications of different aerosol species to direct radiative forcing and

atmospheric heating rate. Atmos. Environ. 241, 117820. https://doi.org/10.1016/j.atmosenv.2020.117820.
Srivastava, A.K., Bhoyar, P.D., Kanawade, V.P., Devara, P.C.S., Thomas, A., Soni, V.K., 2021a. Improved air quality during COVID-19 at an urban megacity over the Indo-Gangetic Basin: from stringent to relaxed lockdown phases. Urban Clim. 36, 100791. https://doi.org/10.1016/j.uclim.2021.100791.
Srivastava, A.K., Thomas, A., Hooda, R.K., Kanawade, V.P., Hyvärinen, A.P., Bisht, D.S., et al., 2021b. How secondary inorganic aerosols from Delhi influence aerosol optical and radiative properties at a downwind sub-urban site over Indo-Gangetic Basin? Atmos. Environ. 248, 118246. https://doi.org/10.1016/j.atmosenv.2021.118246.
Stein, A.F., Draxler, R.R., Rolph, G.D., Stunder, B.J.B., Cohen, M.D., Ngan, F., 2016. NOAA's HYSPLIT atmospheric transport and dispersion modeling system. Bull. Am. Meteorol. Soc. 96, 2059–2077. https://doi.org/10.1175/BAMS-D-14-00110.1.
Storelvmo, T., Leirvik, T., Lohmann, U., Phillips, P.C.B., Wild, M., 2016. Disentangling greenhouse warming and aerosol cooling to reveal Earth's climate sensitivity. Nat. Geosci. 9, 286–289. https://doi.org/10.1038/ngeo2670.
Thamban, N.M., Tripathi, S.N., Moosakutty, S.P., Kuntamukkala, P., Kanawade, V.P., 2017. Internally mixed black carbon in the Indo-Gangetic Plain and its effect on absorption enhancement. Atmos. Res. 197, 211–223. https://doi.org/10.1016/j.atmosres.2017.07.007.
Thomas, A., Sarangi, C., Kanawade, V.P., 2019. Recent increase in winter hazy days over Central India and the Arabian Sea. Sci. Rep. 9, 17406. https://doi.org/10.1038/s41598-019-53630-3.
Tobler, A., Bhattu, D., Canonaco, F., Lalchandani, V., Shukla, A., Thamban, N.M., et al., 2020. Chemical characterization of PM2.5 and source apportionment of organic aerosol in New Delhi, India. Sci. Total Environ. 745, 140924. https://doi.org/10.1016/j.scitotenv.2020.140924.
Torres, O., Tanskanen, A., Veihelmann, B., Ahn, C., Braak, R., Bhartia, P.K., et al., 2007. Aerosols and surface UV products from Ozone Monitoring Instrument observations: an overview. J. Geophys. Res. Atmos. 112. https://doi.org/10.1029/2007jd008809.
Torres, O., Ahn, C., Chen, Z., 2013. Improvements to the OMI near-UV aerosol algorithm using A-train CALIOP and AIRS observations. Atmos. Meas. Tech. 6, 3257–3270. https://doi.org/10.5194/amt-6-3257-2013.